High activity of brookite TiO_2 nanoparticles in the photocatalytic abatement of ammonia in water

Marco Altomare[a], Maria Vittoria Dozzi[a], Gian Luca Chiarello[a], Agatino Di Paola[b], Leonardo Palmisano[b], Elena Selli[a,*]

[a] *Dipartimento di Chimica, Università degli Studi di Milano, via Golgi 19, I-20133 Milano, Italy*

[b] *Dipartimento di Energia, Ingegneria dell'Informazione e Modelli Matematici, Università degli Studi di Palermo, Viale delle Scienze, I-90128 Palermo, Italy*

A B S T R A C T

The effects of the TiO_2 crystal structure and its surface modification with Pt nanoparticles on the photocatalytic oxidation of NH_3 in the aqueous phase were studied with home-made TiO_2 photocatalyst powders synthesized by a thermo-hydrolysis approach that allowed a fine control of the crystallographic phase composition. Ammonia conversion and the selectivity toward mildly oxidized N_2 and highly oxidized nitrite and nitrate anions were monitored during the runs. Pure brookite powders modified by Pt nanoparticles, deposited either from a colloidal suspension or by deposition-precipitation, were found to be the most efficient photocatalysts in NH_3 degradation, with a desired good selectivity toward innocuous N_2. The photo-activity in NH_3 oxidation was correlated to the crystallographic features of the investigated TiO_2-based materials, also taking into account the effects induced on the reaction paths by the presence of Pt nanoparticles on TiO_2.

Keywords: Photocatalysis; TiO_2; Brookite; Thermo-hydrolysis; Ammonia oxidation

* Corresponding author at: Dipartimento di Chimica, Università degli Studi di Milano, via Golgi 19, I-20133 Milano, Italy. Tel.: +39 02 503 14237; fax: +39 02 503 14300.

E-mail address: elena.selli@unimi.it (E. Selli).

1. Introduction

Livestock manure improves the quality of soil and is widely used along with chemical fertilizers to boost agricultural productivity. However, its overuse generates a dangerous accumulation of nitrogen in soil and groundwater which accelerates eutrophication phenomena, leads to dissolved oxygen depletion, increasing the biological oxygen demand, and presents acute toxicity to human health [1]. In such a situation, mandatory is the identification of solutions ensuring suitable disposal of nitrogen in organics, to be applied especially in areas with intensive agricultural activity.

Several technologies have been attempted to solve this problem, including biological processes (with nitrification-denitrification cycles), breakpoint chlorination, ion exchange, air stripping and chemical oxidation [2-4]. These processes ensure only a partial removal of NH_3 and other nitrogen-containing pollutants, and also accumulate them into other streams that then require further treatments to attain the effective elimination of all toxic species.

In this scenario, the photocatalytic oxidation of aqueous NH_3 can be regarded as a promising way to detoxify livestock manure-containing effluents by a single-step process. The first report on this application dates back to 1979, when Mozzanega *et al.* studied the decomposition of NH_3 on anatase TiO_2 under UV light irradiation [5]. Since then, several studies followed, which showed that TiO_2 represents the most promising photocatalyst for such reaction, since the oxidizing species efficiently photo-produced on its surface are able to oxidize NH_3, mainly into nitrite and nitrate ions [6-8], which, however, are also noxious. Thus, the most desirable way to completely remove nitrogen-containing wastes is the selective photocatalytic oxidation of NH_3 into innocuous N_2.

Therefore, the mechanism of NH_3 photocatalytic oxidation needs to be investigated by taking into account the distribution of the final reaction products [9-18]. Some of us recently systematically explored the influence that different experimental conditions have on the photocatalytic abatement of NH_3 in aqueous suspensions and on the selectivity toward its oxidation products [19]. The deposition of metal nanoparticles on TiO_2 was also investigated [20], focusing on the effects of the type/amount of metal on the reaction pathways and product selectivity.

In the present work we report an investigation on the effects that the TiO_2 crystalline structure has on the photocatalytic oxidation of NH_3. Noteworthy, whereas huge attention has been given to the photocatalytic properties of the anatase and rutile TiO_2 polymorphs, the brookite phase started to gain attention only recently, when synthetic routes at mild temperature and pressure were developed [21,22]. Hence, in the present work photocatalytic TiO_2 materials were synthesized by a simple thermo-hydrolysis approach that allowed to finely control the crystalline composition of TiO_2 [23,24]. We found that pure brookite powders exhibit remarkable photoactivity in NH_3 photodegradation, especially when modified with Pt nanoparticles deposition, together with good selectivity toward N_2.

2. Experimental

2.1. Photocatalysts preparation

Home-made anatase (A), brookite (B) and rutile (R) TiO_2 powders were synthesized by the already described thermo-hydrolysis process [23,24], starting from titanium tetrachloride (Fluka, 98%). Briefly, for anatase synthesis 10 mL of $TiCl_4$ were slowly added

to 50 mL of distilled water at room temperature under continuous stirring. After *ca*. 20 min, the resulting clear solution was diluted with water up to a 1:50 $TiCl_4$:H_2O volume ratio and then boiled for 2 h. A milky white anatase dispersion was produced by this way.

Brookite and rutile powders were obtained as follows. 10 mL of $TiCl_4$ were added dropwise to a solution containing 420 mL of water and 160 mL of concentrated hydrochloric acid at room temperature under stirring. Then the solution was heated in a closed bottle and aged for 48 h in an oven at 100 °C. The resultant precipitate contained a brookite-rutile mixture. Pure brookite was separated by peptization through several cycles of supernatant removal followed by water addition up to the initial volume. After a few washings, a dispersion of brookite particles formed, while the rutile phase remained as precipitate [25] and could thus be separated. After removing the supernatant liquid, the obtained powders were collected and dried *in vacuo* at 55 °C.

Two different methods were employed to deposit Pt nanoparticles on the TiO_2 powders. Preformed Pt nanoparticles (NPs) stabilized by *n*-dodecyl trimethyl ammonium chloride were deposited from colloidal suspensions on TiO_2 by means of the already described procedure [24,26,27]. By this way Pt NP deposition occurs at room temperature, thus preventing any crystallographic and morphological modification of the TiO_2 polymorphs. Briefly, the proper amount of metal precursor (*i.e.*, hexachloroplatinic acid) was dissolved in an aqueous solution containing the surfactant (40:1 surfactant to Pt molar ratio). A Pt colloidal suspension was then obtained by adding a large excess of $NaBH_4$ as reducing agent. Afterwards, an aliquot of the colloidal suspension was added under vigorous stirring to a previously sonicated water suspension containing the required amount of photocatalyst powder. Finally, the so obtained powder was recovered, washed and dried overnight in

oven at 70 °C. The nominal Pt NP loading attained by this way was always 1 wt.% with respect to the TiO_2 mass. Pristine and Pt-modified samples were labeled as "P" and "Pt(C)/P", respectively, with P = A, B and R. P25 TiO_2, from Degussa-Evonik, was used as anatase-rutile mixed phase reference material.

Alternatively, a modified version of the well-known Deposition-Precipitation technique [28,29] was employed to deposit Pt NPs on home-made A, R and B and on P25 TiO_2. In this case, the required amount of TiO_2 was added to an aqueous solution containing H_2PtCl_6 (Pt content 0.1 g L^{-1}) and urea (0.42 M). The suspension, thermostated at 80 °C, was vigorously stirred for 4 h, until pH 8 was reached. The slurry was then centrifuged and the recovered powder was re-suspended in water and reduced by addition, under stirring, of a large excess of $NaBH_4$. The suspension color turned from white to grey, confirming the reduction of Pt(IV) to metallic Pt. The so-obtained powder was repeatedly washed with water until the chloride ions content in the supernatant was below 1 ppm and finally dried at 70 °C overnight. These Pt/TiO_2 materials were labeled as "Pt(DP)/P". Their nominal Pt loading was fixed at 0.5 wt.%. ICP analysis, performed by using a Thermo Electron ICAP 6300 after microwave digestion of the photocatalysts in a 3:1 HCl/HNO_3 mixture, confirmed that their actual Pt content was 0.486 wt.% in Pt(DP)/A, 0.467 wt.% in Pt(DP)/B and 0.364 wt.% in Pt(DP)/R.

Most of the chemicals were purchased from Sigma-Aldrich and used as received. Ultra-pure water supplied by a Millipore Direct-Q 3 water purification system was employed to prepare all solutions.

2.2. Photocatalysts characterization

X-ray powder diffraction (XRPD) patterns were recorded on a Philips PW3020 powder diffractometer using the Cu Kα radiation (λ = 1.54056 Å). Quantitative phase analysis was made by the Rietveld refinement method using the "Quanto" software. The specific surface area (BET area) of the powders was measured by N_2 adsorption/desorption at 77 K in a Micromeritics ASAP 2010 apparatus, after out-gassing *in vacuo* at 300 °C for at least 6 h. UV-vis diffuse reflectance spectra of the photocatalyst powders were recorded with a Lambda 19 Perkin Elmer spectrophotometer equipped with an integrating sphere and then converted into absorption spectra [30].

2.3. Photocatalytic tests

The set-up and analytical methods used in this work have already been described [19,20]. The photo-reactor consisted of a 1.1 L cylindrical Pyrex batch vessel, thermostated at 30 °C by means of an external cooling water jacket. The top of the reactor housed an immersion UVA 25 W Jelosil HG100 mercury arc lamp, emitting in the 310-400 nm wavelength range (λ_{max} ~ 365 nm). The irradiation intensity within the photo-reactor was 1.69×10^{-6} Einstein s^{-1}, according to ferrioxalate actinometry.

The TiO_2 aqueous suspensions were sonicated for 15 min, followed by NH_3 addition (initial nitrogen concentration 100 ppm, *ca.* 7 mM) and stirring in the dark for 5 min, until a stable pH was attained (always around 10 - 10.5). Ammonia aqueous solutions were prepared from a 28-30 wt.% NH_3 stock solution. The immersion lamp was switched on at least 15 min before starting the runs and was introduced into the photo-reactor only when its emission intensity was constant (*ca*. 4 mW cm^{-2}, measured by a Jelosil UVA-meter).

The irradiated suspensions contained a fixed photocatalyst amount (0.1 g L^{-1}) and were stirred at constant rate during the runs. Air was continuously bubbled in the photo-reactor at 150 mL min^{-1}. At regular time intervals, 10 mL samples of the reaction suspension were withdrawn and centrifuged. The amount of residual NH_3 (converted into non-volatile NH_4^+ salt by acidification with a H_3PO_4 aqueous solution) and of photocatalytically produced NO_2^- and NO_3^- ions in the supernatant were determined by ion chromatography employing a Metrohm 761 Compact ion chromatograph with conductivity detection. A certified Multianion Standard Solution (Fluka) was used for calibration. The photocatalytic runs lasted 6 h. Some of them were repeated to test their reproducibility.

The amount of NH_3 stripped by air bubbling during the runs was evaluated by conveying the gas stream from the photo-reactor into a flask filled with 5 mM H_3PO_4 aqueous solution (ammonia trap). The concentration of NH_4^+ ions in the trap was analyzed by ion chromatography at the end of the runs and accounted for when evaluating the amount of photocatalytically abated NH_3. Overall, the amount of NH_3 stripped during the 6 h-long runs never exceeded 2.5 % of the initial NH_3 content. Moreover, previous photo-acoustic spectroscopy measurements proved that nitrogen-containing gaseous species such as NO, NO_2 and N_2O were not produced during the runs [19].

3. Results and discussion

3.1. Photocatalyst characterization

The physico-chemical features of the TiO_2 photocatalysts investigated in the present work are summarized in Table 1. XRD analysis (Fig. 1) shows that home-made B consisted of 100% single-phase brookite, whilst home-made A and R were not pure anatase and rutile

samples, but also contained not negligible amounts of brookite. The average crystallite size D_{XRD} of the materials was calculated by the Scherrer equation from the width of the most intense TiO_2 reflections (at 2 θ = 25.4° for anatase, 27.5° for rutile and 30.7° for brookite), obtained as the ratio between the peak area and the peak intensity, evaluated by signal fitting with a Gaussian function. Home-made photocatalysts were characterized by an average grain size lower than 10 nm, *i.e.* smaller than that of P25 crystallites. BET analysis evidenced that sample A, mainly consisting of anatase phase, and sample B (pure brookite) had surface area larger than that of sample R (mainly rutile) and of P25 TiO_2 (see Table 1). Both surface area and phase composition did not significantly change after Pt deposition.

The UV-vis absorption spectra of the home-made naked photocatalysts can be compared in Fig. 2. As expected, sample R, mainly consisting of rutile, exhibits the most red-shifted absorption onset (at *ca*. 420 nm), due to its slightly smaller band gap with respect to anatase and brookite. On the other hand, sample A (mainly anatase) absorbs light below *ca*. 400 nm and pure brookite B exhibits the most hypsochromically-shifted absorption, with an absorption threshold at wavelengths lower than 400 nm. Upon Pt NPs deposition the powders turned from white into light grey. Their band gap absorption onsets did not change compared to their naked counterparts, whereas a broad and featureless absorption appeared in the visible region due to the presence of Pt NPs, as already observed in the case of P25 TiO_2 [20].

3.2. Photocatalytic oxidation of NH_3

Previous studies carried out employing the same photo-reactor and experimental set up evidenced that NH_3 conversion (X_{NH_3}) and the selectivity (S_Y) toward the photo-oxidation

products (Y = N_2, NO_2^- or NO_3^-) are largely affected by the operating conditions and experimental parameters [19,20]. Since not only NH_3, but also NO_2^- and NO_3^- ions are noxious, NH_3 photocatalytic oxidation was investigated to identify the experimental conditions, which ensure high X_{NH_3} values together with high selectivity S_{N_2} toward innocuous dinitrogen.

Table 2 reports the ammonia conversion X_{NH_3} and the selectivity S_Y values obtained in the present study after 6 h-long runs employing the here investigated photocatalysts, either naked or Pt-modified by the colloidal method, Pt(C)/P, or by deposition precipitation, Pt(DP)/P.

The effects of the TiO_2 crystalline phase on NH_3 photocatalytic conversion when naked TiO_2 photocatalysts were employed can be better appreciated in Fig. 3, together with the effects induced by Pt NPs deposition on the different photocatalyst samples. Home-made powders were clearly less active than P25. In particular, a rather poor ammonia conversion X_{NH_3} was attained with R, that can partly be ascribed to the relatively fast charge carriers recombination, typical of the rutile phase, usually correlated to its relatively low conduction band position, preventing efficient electron transfer to O_2 [31]. On the other hand, P25 powders showed significantly higher X_{NH_3} compared also to home-made anatase (A) and brookite (B), although these latter exhibit a higher surface area (Table 1). Such relatively high photo-activity of P25 is generally attributed to the presence of anatase/rutile hetero-junctions in its structure, resulting in more efficient charge carrier separation [32].

Also the effects of Pt NPs deposition on the different photocatalysts can better be appreciated in Fig. 3. The presence of Pt NPs on the semiconductor oxide led to an increase

of ammonia conversion X_{NH3} for all photocatalysts, as already observed for P25 [20]. This effect is attributed to a better charge carrier separation consequent to the ability of noble metal nanoparticles to efficiently capture conduction band electrons [33], thus making valence band holes more readily available for oxidation reactions. Furthermore, the photoactivity scale largely changed upon Pt NPs deposition, compared to that observed for the corresponding naked samples. In particular, pure brookite B became the most active material upon Pt NPs deposition, independently of the employed deposition method. In fact, the highest ammonia conversion X_{NH3} values were attained with both Pt(C)/B and Pt(DP)/B photocatalysts, together with reasonably good S_{N2} values (see Fig. 3 and Table 2). On the other hand, the photo-activity of Pt/R in terms of ammonia conversion was ca. 3 times that of naked R, but still remained very poor compared to those of the other Pt-modified samples.

The largest photoactivity increment upon Pt NPs deposition was clearly obtained in the case of home-made photocatalysts A and especially B. In fact, X_{NH3} values more than twice and almost three times higher, respectively, than those measured with the corresponding naked materials were obtained, while the increment observed in the case of P25 was relatively smaller. This might be a consequence of the intrinsically good charge carriers separation properties of P25, which are relatively less improved by the presence of Pt NPs, able to efficiently capture conduction band electrons and to ensure a more effective electron transfer to adsorbed O_2.

Fig. 3 also evidences that the increase in ammonia conversion does not exhibit any clear dependence on the way Pt NPs were deposited on the photocatalyst surface (*i.e.* either by

the colloidal method or by deposition-precipitation), nor on the amount of deposited metal (either 1 or 0.5 wt.%, respectively). Among the different photocatalysts investigated in the present study, pure brookite B thus appears to have maximum beneficial effect on photoactivity by Pt NPs deposition, especially if carried out by the modified deposition-precipitation method employed in this work (see Fig. 3 and Table 2).

The high X_{NH_3} values and the origin of different S_{N_2} values obtained with Pt-modified A and B can better be explained by taking into account the concentration profiles of the reactant, intermediate and final products of ammonia photocatalytic oxidation, trying to get information on the role that the Pt co-catalyst may have in modifying the rate of the different ammonia photo-oxidation pathways.

Fig. 4 shows the concentration of NH_3 and of the NO_2^- and NO_3^- ions as a function of irradiation time during ammonia photocatalytic oxidation on naked brookite, anatase and P25, as well as on their Pt-modified (colloidal method) counterparts. First of all, negligibly low amounts of NO_3^- ions were produced with naked A and B, whereas NO_3^- ions were produced at a continuously increasing rate on naked P25. This resulted in a higher selectivity (> 40%) toward N_2 for all these samples (Table 2) and in extremely low $S_{NO_3^-}$ values for A and B, but not for P25. The rates of both NH_3 degradation and NO_2^- formation were rather steady over time in the case of photocatalysts A and B, but not for P25.

The photocatalytic oxidation of NH_3 is expected to occur on the photocatalyst surface through a valence band holes (or $^{\bullet}OH$ radicals) – mediated mechanism implying the mild oxidation of adsorbed NH_3 molecules to form $-(NH_2)_{ox}$ intermediates [20]. These latter may undergo further oxidation to form N_2 molecules or NO_2^- anions. Photocatalytic N_2

evolution, requiring two nitrogen-containing species close to each other on the photocatalyst surface, and proceeding with relatively high selectivity in the case of A and B photocatalysts, may result from a sort of surface disproportionation reaction involving adsorbed ammonia and the nitrite ions [34], especially if these latter do not undergo further oxidation to NO_3^-, as is the case of photocatalysts A and B.

The concentration *vs.* time profiles of NH_3, NO_2^- and NO_3^- recorded during the photocatalytic runs with the Pt-modified photocatalysts, also shown in Fig. 4, evidence remarkably higher rates of both NH_3 degradation and NO_3^- formation with respect to the runs carried out with the corresponding naked photocatalysts, as a consequence of the already mentioned more effective photoproduced electron-hole separation induced by the presence of noble metal NPs [20,33]. Moreover, nitrate anions formed from the very beginning of the photocatalytic runs and the nitrite ions concentration profile did not increase continuously, as in the case of the runs carried out with naked A and B, but it reached a maximum value and then decreased. Thus, the formation of nitrate ions appears to occur through two parallel paths, *i.e.* either *i*) through two consecutive reactions [19,20], the first one consisting in the formation of NO_2^- from NH_3, followed by NO_2^- further oxidation into NO_3^- ions; or *ii*) through the direct oxidation of ammonia into NO_3^- ions, on the photocatalyst surface. Path *ii*) is clearly active only in the case of the Pt-modified materials and should be related to the higher amount of surface oxidizing species, such as the $^{\bullet}O_2^-$ radicals produced by dioxygen reduction, which is activated by Pt nanoparticles, and the $^{\bullet}OH$ radicals resulting from both the increased availability of valence band holes and the increased electron transfer rate mediated by Pt NPs.

Interestingly, as shown in Fig. 5, when naked B was employed as photocatalyst, the selectivity to N_2, S_{N_2}, increased during the runs with a simultaneous mirroring decrease of $S_{NO_2^-}$, indicating nitrite ions as precursors of N_2 photocatalytic evolution. In contrast, S_{N_2} remained nearly constant over the entire reaction with Pt(C)/B (Fig. 5), suggesting that in this case the formation of N_2 and that of nitrite and nitrate ions mainly occur through independent paths. Furthermore, in this case the increase of $S_{NO_3^-}$ occurring during the runs is perfectly mirrored by the decrease of $S_{NO_2^-}$, testifying the almost complete transformation of nitrite into nitrate ions. In the case of naked B, S_{N_2} increased with the increased availability of the nitrite ion precursors during the run, whereas in the case Pt-modified B nitrite ions mainly underwent further oxidation into nitrates.

Therefore, the presence of Pt NPs on the here investigated photocatalysts mainly boosts all oxidation steps, leading to an increase of X_{NH_3} and $S_{NO_3^-}$, but to a decrease of S_{N_2}, N_2 evolution occurring in competition with further NO_2^- oxidation into NO_3^-. The higher increase of X_{NH_3} obtained upon Pt NPs deposition on B compared to A (and to the more intrinsically active P25 TiO_2) can be related to the more negative conduction band edge of brookite [22] (see Fig. 2) providing a larger driving force for the Pt-mediated electron transfer at the interface, with a larger production of radical species that in turn induces more efficient NH_3 oxidation.

4. Conclusions

Intriguing effects concerning the mechanism of NH_3 degradation were observed upon Pt NPs deposition on pure brookite and on (mainly) anatase powders. In particular, NH_3

underwent a mild oxidation reaction, forming N_2 and nitrite ions, when the photocatalytic process was performed with naked brookite or anatase. On the other hand, quite higher photo-efficiency, along with a significant formation of highly oxidized products (*i.e.* nitrate anions), was achieved in the presence of Pt-loaded pure brookite or Pt-loaded anatase.

Overall, the outstanding rates of photocatalytic ammonia degradation obtained with Pt-loaded brookite not only demonstrate that the brookite polymorph represents an efficient photocatalyst for both oxidation and reduction reactions, but also suggests that the photoactivity of pure, undoped TiO_2 is still worth of in depth investigation in relation to its crystallographic features and phase mixtures.

Acknowledgments

The collaboration of Sabrina Brocato in the experimental part of the work is gratefully acknowledged. The research project entitled *Photocatalytic Ammonia Reduction in Manure – PhARM* was funded by the Agriculture Department of Regione Lombardia. This work received financial support also from Cariplo Foundation through the project entitled *Novel photocatalytic materials based on heterojunctions for solar energy conversion*.

References

[1] J. Webb, H. Menzi, B.F. Pain, T.H. Misselbrook, U. Dämmgen, H. Hendriks, H. Döhler, Environ. Pollut. 135 (2005) 399–406.

[2] C.E. Adams, Environ. Sci. Technol. 7 (1973) 696–701.

[3] R.W. Melse, N.W.M. Ogink, W.H. Rulkens, Open Agric. J. 3 (2009) 6–12.

[4] Y.H. Ahn, Process Biochem. 41 (2006) 1709–1721.

[5] H. Mozzanega, J.M. Herrmann, P. Pichat, J. Phys. Chem. 83 (1979) 2251–2255.

[6] A. Bravo, J. Garcia, X. Doménech, J. Peral, J. Chem. Res. (Suppl.) (1993) 376–377.

[7] J. Lee, H. Park, W. Choi, Environ. Sci. Technol. 36 (2002) 5462–5468.

[8] X. Zhu, S.R. Castleberry, M.A. Nanny, E.C. Butler, Environ. Sci. Technol. 39 (2005) 3784–3791.

[9] I. Mikami, S. Aoki, Y. Miura, Chem. Lett. 39 (2010) 704–705.

[10] H. Kominami, H. Gekko, K. Hashimoto, Phys. Chem. Chem. Phys. 12 (2010) 15423–15427.

[11] S. Yamazoe, T. Okumura, T. Tanaka, Catal. Today 120 (2007) 220–225.

[12] J.G. Chang, S.P. Ju, C.S. Chang, H.T. Chen, J. Phys. Chem. C 113 (2009) 6663–6672.

[13] S. Yamazoe, T. Okumura, K. Teramura, T. Tanaka, Catal. Today 111 (2006) 266–270.

[14] S. Yamazoe, T. Okumura, H. Hitomi, T. Shishido, T. Tanaka, J. Phys. Chem. C 111 (2007) 11077–11085.

[15] K. Teramura, T. Tanaka, S. Yamazoe, K. Arakaki, T. Funabiki, Appl. Catal. B Environ. 53 (2004) 29–36.

[16] H.H. Ou, M.R. Hoffmann, C.H. Liao, J.H. Hong, S.L. Lo, Appl. Catal. B Environ. 99 (2010) 74–80.

[17] M. Kaneko, H. Ueno, R. Saito, J. Nemoto, Catal. Lett. 137 (2010) 156–162.

[18] T. Tanaka, K. Teramura, K. Arakaki, T. Funabiki, Chem. Commun. (2002) 2742–2743.

[19] M. Altomare, G.L. Chiarello, A. Costa, M. Guarino, E. Selli, Chem. Eng. J. 191 (2012) 394–401.

[20] M. Altomare, E. Selli, Catal. Today 209 (2013) 127–133.

[21] A. Pottier, C. Chanéac, E. Tronc, L. Mazerolles, J.P. Jolivet, J. Mater. Chem. 11 (2001) 1116–1121.

[22] A. Di Paola, M. Bellardita, L. Palmisano, Catalysts 3 (2013) 36–73.

[23] A. Di Paola, M. Bellardita, R. Ceccato, L. Palmisano, F. Parrino, J. Phys. Chem. C 113 (2009) 15166–15174.

[24] G.L. Chiarello, A. Di Paola, L. Palmisano, E. Selli, Photochem. Photobiol. Sci. 10 (2011) 355–360.

[25] A. Di Paola, G. Cufalo, M. Addamo, M. Bellardita, R. Campostrini, M. Ischia, R. Ceccato, L. Palmisano, Colloids Surf. A: Physicochem. Eng. Aspects 317 (2008) 366–376.

[26] A.Q. Wang, C.M. Chang, C.Y. Mou, J. Phys. Chem. B 109 (2005) 18860–18867.

[27] G.L. Chiarello, M.H. Aguirre, E. Selli, J. Catal. 273 (2010) 182–190.

[28] R. Zanella, S. Giorgio, C.R. Henry, C. Louis, J. Phys. Chem. B 106 (2002) 7634–7642.

[29] M.V. Dozzi, L. Prati, P. Canton, E. Selli, Phys. Chem. Chem. Phys. 11 (2009) 7171–7180.

[30] M.V. Dozzi, B. Ohtani, E. Selli, Phys. Chem. Chem. Phys. 13 (2011) 18217–18227.

[31] C. Bernardini, G. Cappelletti, M.V. Dozzi, E. Selli, J. Photochem. Photobiol. A: Chem. 211 (2010) 185–192.

[32] D.C. Hurum, K.A. Gray, T. Rajh, M.C. Thurnauer, J. Phys. Chem. B 109 (2005) 977–980.

[33] A. Naldoni, M. D'Arienzo, M. Altomare, M. Marelli, R. Scotti, F. Morazzoni, E. Selli, V. Dal Santo, Appl. Catal. B Environ. 130–131 (2013) 239–248.

[34] D.K. Lee, J.S. Cho, W.L. Yoon, Chemosphere 61 (2005) 573–578.

Table 1

BET specific surface area (SSA), phase composition, assuming the absence of amorphous material, and average crystallite diameter D_{XRD}, from XRD analysis, of the TiO_2 photocatalysts tested in NH_3 photocatalytic oxidation.

Sample	SSA (m^2 g^{-1})	Crystallographic phase (%)			D_{XRD} (nm)
		Anatase	Rutile	Brookite	
P25	48	80	20	-	25
A	180	82	-	18	3.5
R	25	-	88	12	5.6
B	80	-	-	100	8.1

.

Table 2

Ammonia conversion (X_{NH_3}) and product selectivity of naked and Pt-modified photocatalysts.

Sample	X_{NH_3} (%)	Selectivity (%)		
		NO_2^-	NO_3^-	N_2
P25	25.7	31.2	26.9	41.9
A	15.5	44.0	4.0	52.0
R	3.1	71.5	8.3	20.2
B	17.6	58.2	1.3	40.5
Pt(C)/P25	43.2	23.1	48.7	28.2
Pt(C)/A	33.4	25.8	42.2	32.0
Pt(C)/R	10.3	54.4	12.8	32.8
Pt(C)/B	48.7	12.4	56.4	31.2
Pt(DP)/P25	39.1	54.2	27.1	18.7
Pt(DP)/A	37.5	42.2	35.7	22.1
Pt(DP)/R	8.8	38.6	15.2	46.2
Pt(DP)/B	51.4	26.0	47.4	26.6

Figure captions

Fig. 1. XRD patterns of the investigated naked TiO_2 samples and position of the diffraction peaks of the TiO_2 crystalline phases.

Fig. 2. UV-vis absorption spectra of rutile (R), anatase (A) and brookite (B) photocatalysts (upper panel) and band edges of pure anatase, brookite, and rutile at pH 7 from ref. [23] (lower panel).

Fig. 3. Photocatalytic ammonia conversion (X_{NH3}) attained after 6 h with the photocatalysts either naked (white) or modified by Pt NPs deposition, both from a colloidal suspension, Pt(C) (black) or by deposition-precipitation, Pt(DP) (grey).

Fig. 4. Concentration profiles of NH_3, NO_2^- and NO_3^- during ammonia photocatalytic oxidation on naked or Pt NPs-modified photocatalysts (Pt NPs deposition from colloidal suspension).

Fig. 5. Ammonia conversion X_{NH3} and selectivities to N_2, NO_2^- and NO_3^- during the runs carried out with pure brookite B and with Pt NPs modified brookite Pt(C)/B.

Fig. 1.

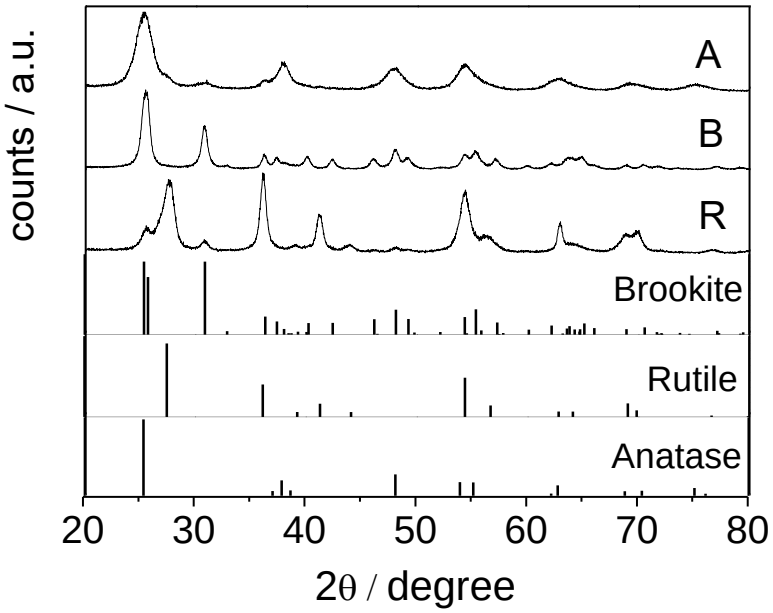
counts / a.u.
A
B
R
Brookite
Rutile
Anatase
20
30
40
50
60
70
80
2θ / degree

Fig. 2.

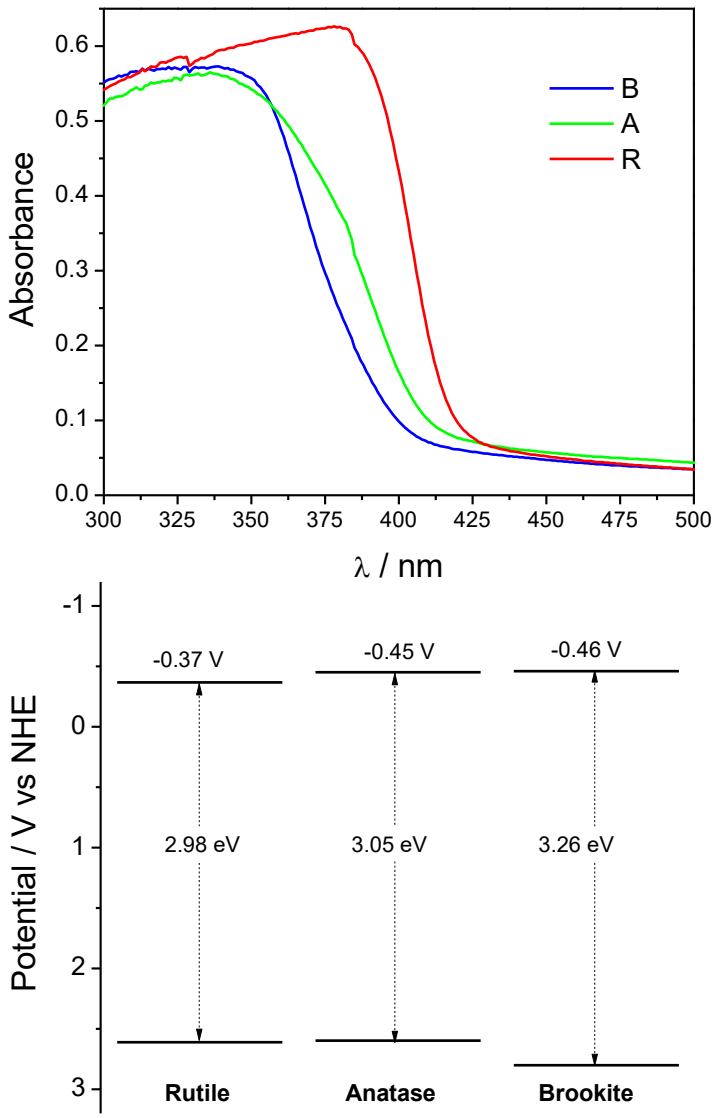
Absorbance
λ / nm
B
A
R
Potential / V vs NHE
-0.37 V
-0.45 V
-0.46 V
2.98 eV
3.05 eV
3.26 eV
Rutile
Anatase
Brookite

Fig. 3.

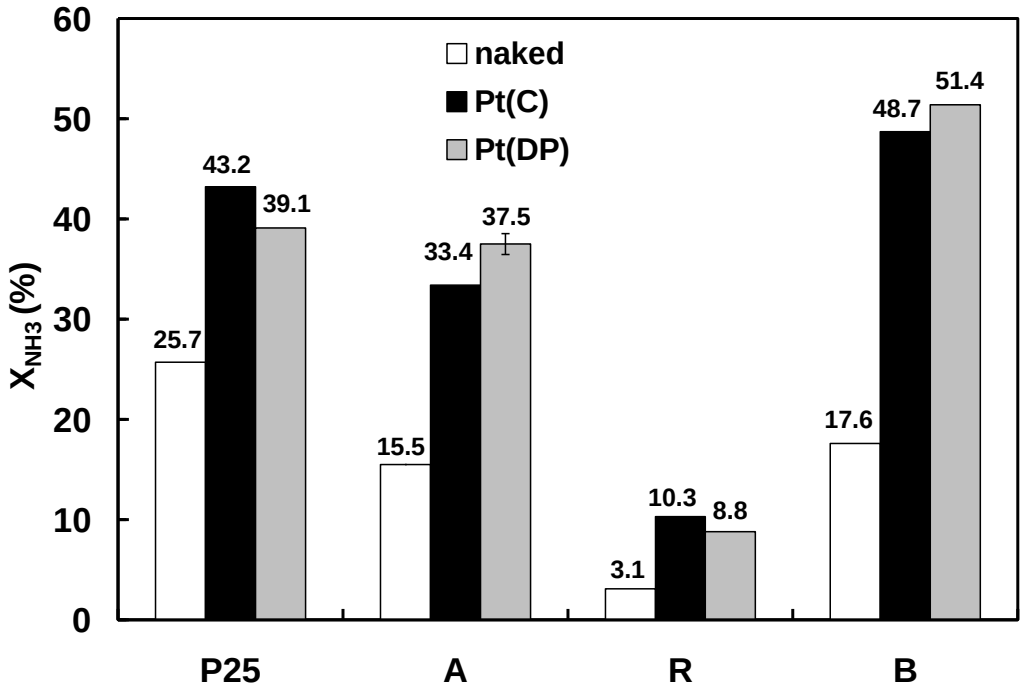
60
50
40
30
20
10
0
X_{NH3} (%)
naked
Pt(C)
Pt(DP)
25.7
43.2
39.1
15.5
33.4
37.5
3.1
10.3
8.8
17.6
48.7
51.4
P25
A
R
B

Fig. 4.

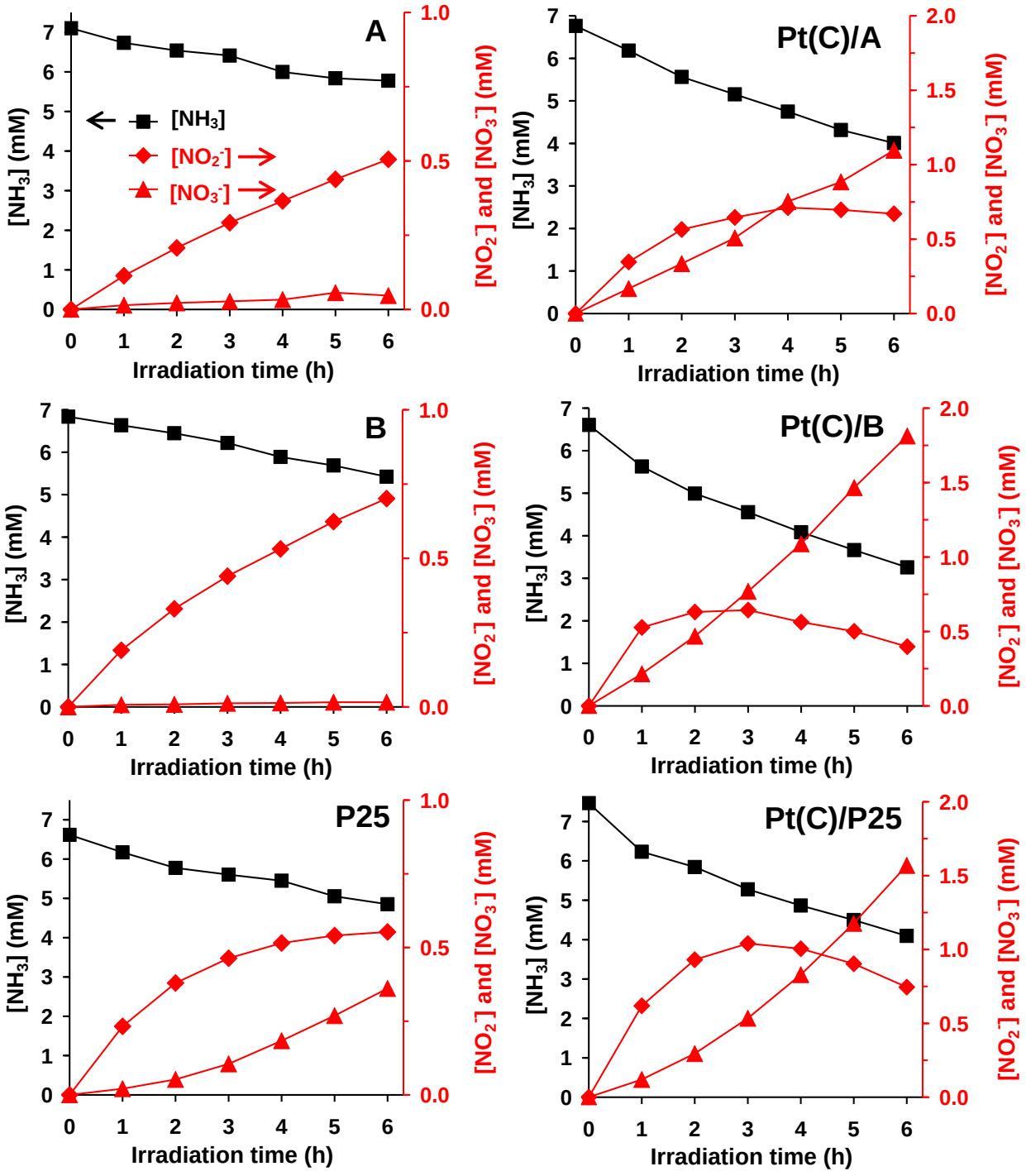
A
Pt(C)/A
B
Pt(C)/B
P25
Pt(C)/P25
[NH3]
[NO2-]
[NO3-]
[NH3] (mM)
[NO2-] and [NO3-] (mM)
Irradiation time (h)

Fig. 5.

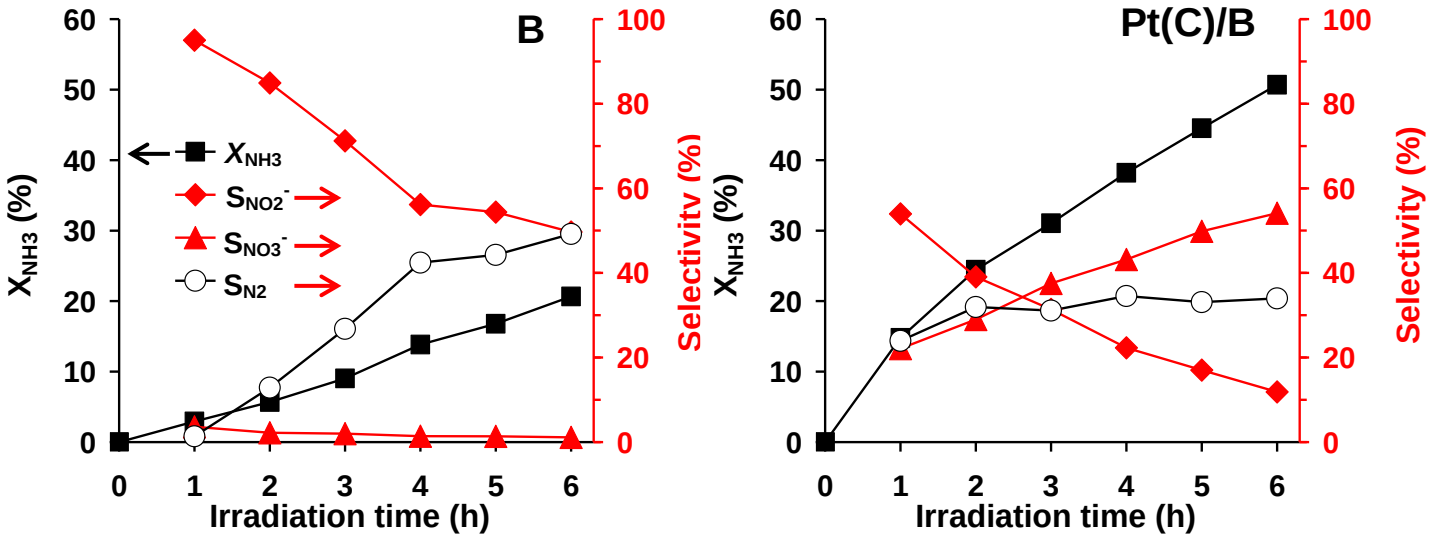
B
Pt(C)/B
X_{NH3} (%)
Selectivity (%)
Irradiation time (h)
X_{NH3}
S_{NO2^-}
S_{NO3^-}
S_{N2}
0
10
20
30
40
50
60
0
20
40
60
80
100
0
1
2
3
4
5
6